Received: 29 May 2024 | Revised: 1 August 2024 | Accepted: 5 August 2024

DOI: 10.1002/glia.24607

GLIA

WILEY

RESEARCH ARTICLE

Astrocytic Ca^{2+} activation by chemogenetics mitigates the effect of kainic acid-induced excitotoxicity on the hippocampus

Nira Hernández-Martín[1,2] | María Gómez Martínez[1] | Pablo Bascuñana[1,2] | Rubén Fernández de la Rosa[1,3] | Luis García-García[1,2,4] | Francisca Gómez[1,2,4] | Maite Solas[5] | Eduardo D. Martín[6] | Miguel A. Pozo[1,2,7]

[1]Instituto Pluridisciplinar, Universidad Complutense de Madrid, Madrid, Spain

[2]Instituto de Investigación Sanitaria San Carlos (IdISSC), Hospital Clínico San Carlos, Madrid, Spain

[3]Bioimac, Universidad Complutense de Madrid, Madrid, Spain

[4]Departamento de Farmacología, Farmacognosia y Botánica, Facultad de Farmacia, Universidad Complutense de Madrid, Madrid, Spain

[5]Facultad de Farmacia, Universidad de Navarra, Pamplona, Spain

[6]Instituto Cajal, CSIC, Madrid, Spain

[7]Facultad de Medicina, Universidad Complutense de Madrid, Madrid, Spain

Correspondence
Nira Hernández-Martín, PET Center, Department of Radiology & Biomedical Imaging, Yale University School of Medicine, 333 Cedar Street, New Haven, CT 06510, USA.
Email: nira.hernandezmartin@yale.edu

Present addresses
Nira Hernández-Martín, PET Center, Department of Radiology & Biomedical Imaging, Yale University School of Medicine, New Haven, Connecticut, USA; and María Gómez Martínez, Radiochemistry and Nuclear Imaging, CIC biomaGUNE, Gipuzkoa, Spain.

Funding information
Agencia Estatal de Investigación; Ministerio de Ciencia, Innovación y Universidades, Grant/Award Numbers: PDI2019-106968RB-100, PID2020-116327GB-100, SAF2017-87619-P; Instituto de Salud Carlos III, Grant/Award Number: CP21/00020; Universidad Complutense de Madrid; Comunidad de Madrid

Abstract

Astrocytes play a multifaceted role regulating brain glucose metabolism, ion homeostasis, neurotransmitters clearance, and water dynamics being essential in supporting synaptic function. Under different pathological conditions such as brain stroke, epilepsy, and neurodegenerative disorders, excitotoxicity plays a crucial role, however, the contribution of astrocytic activity in protecting neurons from excitotoxicity-induced damage is yet to be fully understood. In this work, we evaluated the effect of astrocytic activation by Designer Receptors Exclusively Activated by Designer Drugs (DREADDs) on brain glucose metabolism in wild-type (WT) mice, and we investigated the effects of sustained astrocyte activation following an insult induced by intrahippocampal (iHPC) kainic acid (KA) injection using 2-deoxy-2-[^{18}F]-fluoro-D-glucose (^{18}F-FDG) positron emission tomography (PET) imaging, along with behavioral test, nuclear magnetic resonance (NMR) spectroscopy and histochemistry. Astrocytic Ca^{2+} activation increased the ^{18}F-FDG uptake, but this effect was not found when the study was performed in *knock out* mice for type-2 inositol 1,4,5-trisphosphate receptor ($Ip3r2^{-/-}$) nor in *floxed* mice to abolish glucose transporter 1 (GLUT1) expression in hippocampal astrocytes ($GLUT1^{\Delta GFAP}$). Sustained astrocyte activation after KA injection reversed the brain glucose hypometabolism, restored hippocampal function, prevented neuronal death, and increased hippocampal GABA levels. The findings of our study indicate that astrocytic GLUT1 function is crucial for regulating brain

glucose metabolism. Astrocytic Ca^{2+} activation has been shown to promote adaptive changes that significantly contribute to mitigating the effects of KA-induced damage. This evidence suggests a protective role of activated astrocytes against KA-induced excitotoxicity.

KEYWORDS
astrocyte, DREADDs, excitotoxicity, FDG PET, metabolism

1 | INTRODUCTION

Astrocytes are the most abundant types of brain cells, and their role is considered pivotal as they are involved in many functions relevant to cells survival, such as maintaining and regulating neuronal glucose metabolism (Attwell et al., 2010; Barros, Brown, & Swanson, 2018; Gordon et al., 2007). Located in a privileged position, in the interface between blood vessels and neurons, astrocytes have specific channels for sensing and transporting glucose. Thus, based on glucose availability and the neuronal energetic requirements, astrocytes are able to control the amount of glucose that enters the brain cells (Marina et al., 2018). In addition, astrocytes are involved in several other processes, including neuroinflammation, reactive gliosis, and glial scarring (Al Sufiani & Ang, 2012). In damaged brain areas, astrocytes undergo molecular and physiological changes that may be related to the onset and progression of neurodegeneration (Sofroniew & Vinters, 2010).

Astrocytes also play a prominent role in regulating glutamate homeostasis (Andersen et al., 2021; Danbolt et al., 2016). Particularly, astrocyte-derived glutamine has a key role in regulation during sustained glutamatergic signaling, as the inhibition of glutamine synthesis in these cells disrupts neurotransmission and brain energy homeostasis (Andersen et al., 2017). An altered astrocyte function may contribute to the excitotoxicity damage induced by glutamate (Provenzano et al., 2023), defined as a condition where the postsynaptic activation of glutamatergic neurons is excessive (Olney, 1971). This may increase the susceptibility to excitotoxicity, leading to a process that ultimately results in the neuronal death (Qian et al., 2011), a hallmark of neurodegenerative diseases (Brandebura et al., 2023; Hynd et al., 2004; Iovino et al., 2020; Sepers & Raymond, 2014; Stoklund Dittlau & Freude, 2024). Moreover, it has been proposed that cellular glutamate-processes, as glutamate storage, synthesis, receptor signaling, uptake, and recycling, are closely related to brain energy metabolism (Andersen et al., 2021).

Positron emission tomography (PET) with 2-deoxy-2-[^{18}F]fluoro-D-glucose (^{18}F-FDG) is an imaging technique that allows to study brain glucose metabolism in a minimal invasive manner. Thus, in the clinical context, ^{18}F-FDG PET has been used to localize the seizure focus on epilepsy patients (Carne et al., 2004; Duncan, 2009) as well as to diagnose dementia-related diseases such as Alzheimer's disease (Garibotto et al., 2017; Mosconi et al., 2009), dementia with Lewy bodies (McKeith et al., 2017), frontotemporal dementia (Dave et al., 2020; Jeong et al., 2005), Parkinson's disease (Meyer et al., 2017), and atypical parkinsonism (Walker et al., 2018). These ^{18}F-FDG PET studies in neurodegenerative diseases show brain glucose hypometabolism as a common feature. ^{18}F-FDG PET studies are also performed in preclinical animal models, including a model of excitotoxicity and epilepsy such as the one induced by intrahippocampal (iHPC) kainic acid (KA), an L-glutamate analogue that produces alterations in excitability and toxicity (Bascuñana et al., 2020; Kornblum et al., 2000; Mirrione et al., 2006) providing real-time insights into biological process over time.

The role of astrocytes on brain glucose metabolism under conditions of damage is yet to be fully elucidated. To address this issue, we used an experimental approach involving Designer Receptors Exclusively Activated by Designer Drugs (DREADDs). DREADDs are adenovirus-associated muscarinic silent receptors that can be transfected into localized areas in the brain and selectively activated using clozapine-N-oxide (CNO). This technique can be used to modulate astrocyte activity by increasing Ca^{2+} signaling, with diverse effects in each brain cell type (Bonder & McCarthy, 2014; Shen et al., 2021). Specifically, activation of Gq G-Protein Coupled Receptors (Gq-GPCR) DREADDs sets in motion an intracellular signaling pathway in which the type-2 inositol 1,4,5-trisphosphate (Ip3) receptors are the final responsible for the intracellular Ca^{2+} concentrations increase (Corkrum et al., 2020; Martin-Fernandez et al., 2017; Petravicz et al., 2008).

Herein, we sought to investigate the potential protective role of astrocyte activation against KA-induced excitotoxicity. We use ^{18}F-FDG PET neuroimaging to assess the effects of chemogenetic astrocyte activation on glucose metabolism in *wild type* (WT) and in genetically modified mice to unveil the molecular mechanism involved in DREADDs activation in astrocytes. In addition, we interrogate the effect of astrocyte modulation after KA-induced damage.

2 | MATERIALS AND METHODS

2.1 | Animals

Adult male WT C57BL/6J mice (4 months-old) were obtained from Charles River Laboratories (Spain). Transgenic mice *knock out* for Ip3 receptors (Ip3r2$^{-/-}$) (Li et al., 2005) were kindly provided by Gertrudis Perea. A conditional *floxed* mice model to ablate the glucose transporter 1 (GLUT1) exclusively in hippocampal astrocytes through *Cre*-mediated recombination (GLUT1$^{\Delta GFAP}$) was used. This last animal was derived from the general GLUT1 ablation hGFAPCreERT2:

GLUT1$^{f/f}$ mice model (Ardanaz et al., 2022). Upon arrival, animals were housed 4/cage in standard cages on a ventilated rack (Tecniplast, Italy) under controlled temperature (22 ± 2°C) and 12 h light/dark cycle, with free access to standard rodent chow (Safe, France) and tap water. Prior to the start of the procedures, animals were allowed to acclimatize to the new housing conditions for at least 1 week to reduce the stress component associated with the procedures. All experiments were performed between 0800 and 1600 h to reduce any circadian cycle influence.

To study the effects of astrocytic Ca^{2+} activation in ^{18}F-FDG uptake, adult male WT mice were injected either with DREADDs (WT/DREADD, $n = 10$) or with a control virus (WT/CONTROL, $n = 12$). Additionally, we injected DREADDs in Ip3r2$^{-/-}$ ($n = 5$) and GLUT1$^{\Delta GFAP}$ ($n = 8$) mice.

To examine the effects of astrocytic Ca^{2+} activation after KA-induced insult all WT mice were injected with DREADDs and then divided into two groups: (i) injection of iHPC KA and (ii) iHPC injection of saline (VEH). These animals were treated with CNO or saline (SAL) from day 1 to day 7 after either KA or VEH injection. Thus, the resulting groups with DREADDs in this experiment were classified as VEH + SAL ($n = 9$), VEH + CNO ($n = 8$), KA + SAL ($n = 8$), and KA + CNO ($n = 8$).

2.2 | Stereotaxic viral injection

Animals were anesthetized under isoflurane (2% in oxygen at flow rate of 1 L/min) and placed in a stereotaxic frame (Stoelting, USA) to perforate the skull at the coordinates corresponding to the allocation of the hippocampal CA1 according to the following bregma coordinates: AP −2.1 mm; LM ±1.6 mm; DV −1.5 mm. DREADDs (pAAV-GFAP-hm3D(Gq)-mCherry Titer: 1.2×10^{13} GC/mL Addgene 50478-AAV5) or control virus (pAAV-GFAP104-mCherry Titer: 1.2×10^{13} GC/mL Addgene 58909-AAV5) diluted in artificial cerebrospinal fluid were injected using a 2 µL, 34-gauge needle Hamilton syringe (Microliter Syringe 7002, Hamilton Company, USA) connected to a stereotaxic microinjector (Stoelting, USA). The injections were performed bilaterally, with a volume of 0.5 µL in each hemisphere at a rate of 0.5 µL/min. At the end of the injection, the needle remained in place for two additional minutes to ensure the proper viral diffusion and to prevent eventual back flow.

For the *floxed* GLUT1$^{\Delta GFAP}$ mice, hippocampal GLUT1 expression was abolished by injecting a GFAPCre virus (AAV2/5-GFAP104-cre-mCherry Titer 2.8×10^{12} GC/mL, 0.5 µL) in the hippocampus along with the DREADDs. Animals were allowed to recover in their cages for 2 weeks before the neuroimaging studies were performed.

2.3 | Intrahippocampal KA injection

Three weeks after the viral injection procedures, a subgroup of animals underwent injection of iHPC KA (0.21 µg in 0.5 µL saline) or vehicle (saline) at a rate of 0.5 µL/min, in the same coordinates of viral injection. KA injection and behavior were evaluated and scored according to the Racine scale (Racine, 1972) to confirm that all animals developed *status epilepticus*. The scale is divided into the following levels: (0) immobility, (1) facial movements and head nodding, (2) convulsive waves through the body or piloerection and erect tail, (3) myoclonic jerks in forelimbs, (4) clonic convulsions in all extremities or falling on one side, and (5) tonic–clonic convulsions in the whole body or falling on the back. Following the occurrence of seizures, the animal may display a lack of mobility, which corresponds to the postictal period. Recovery is indicated when the animal begins to engage in exploratory behaviors.

2.4 | CNO treatment

Acute DREADDs activation was achieved using CNO (3 mg/kg ip, Merck Sigma-Aldrich, Germany). Each animal underwent two PET studies, in which they were injected with either saline or CNO. The order in which the animals received the treatments was varied to avoid the effect of drug interaction. Drugs were injected 10 min prior to ^{18}F-FDG administration, to ensure that the incorporation of the radiotracer matched with the maximum concentration of the drug in blood. To examine the effects of astrocyte activation after glutamate excitotoxicity, chronic astrocyte activation was performed from day 1 to day 7 after KA injection. On day 1, mice were ip injected with CNO at a dose of 3 mg/kg. The following days (2–7) the dose was of 1 mg/kg ip. On experimental days corresponding to PET scans, mice were injected 10 min before ^{18}F-FDG administration.

2.5 | ^{18}F-FDG positron emission tomography imaging

PET/CT (computed tomography) scans were acquired using a small animal PET/CT scanner (Albira ARS PET/CT dual scanner, Bruker, Germany). Dynamic scans were performed to assess changes in ^{18}F-FDG uptake caused by astrocytic Ca^{2+} activation. Animals were anesthetized with isoflurane (2% in oxygen) and catheterized through the tail vein with a 34-gauge needle connected to a cannula. Thereafter, they were introduced into the scan for a 60 min dynamic acquisition. ^{18}F-FDG (approx. 5.55 MBq/200 µL saline, iv, Curium Pharma, Spain) was injected through the cannula 10 s after the beginning of the acquisition. Finally, the CT image was acquired. PET images were reconstructed using maximum likelihood expectation maximization (MLEM) algorithm. The iterative reconstruction of PET data comprises 32 frames of 5×2 s, 4×5 s, 3×10 s, 8×30 s, 5×60 s, 4×300 s, and 3×600 s.

To evaluate the effect of DREADD activation in awake animals, we also performed static PET acquisitions. Each animal had two studies, injected with saline or CNO. To assess brain metabolism after KA injection, each animal was subjected to three image acquisitions: one basal before the KA injection (−1 day) and two after the insult (days 1 and 8). The animals were fasted at least 8 h prior to the study. Animals were injected with ^{18}F-FDG (approx. 5.92 MBq/200 µL ip, saline, Curium Pharma, Spain) and waited for 45 min of awake uptake. Then, the animal was anesthetized with isoflurane (2% in oxygen) and introduced into the scanner where a 20-min PET acquisition and a 10-min CT scan were performed. Blood glucose levels were measured prior to the PET scan.

PET images were automatically fused with each individual CT and were coregistered to Mirrione's brain magnetic resonance imaging (MRI) template (Ma et al., 2005), which includes a selection of volumes of interest (VOIs) according to different brain regions, using PMOD 4.1 software (PMOD Technologies Ltd., Switzerland). Dynamic scans were analyzed using the 2-tissue-compartment (2TC) for ^{18}F-FDG kinetic model. Together with the VOIs of the different brain areas, another spherical VOI of cava vein (1 mm^3) was created to determine the blood input function and its time-activity curve was fitted to a three exponential whole blood model. We calculated the kinetic parameter k_i (1/min), a rate constant that indicates the flow of the radiotracer through the two compartments ($k_i = (K_1 \times k_3)/(k_2 + k_3)$). Static scans were analyzed by percentage of injected dose per cubic centimeter (%ID/cc). Statistical Parametric Mapping 12 software (SPM; Wellcome Trust Center for Neuroimaging, UCL, UK) in MATLAB (The MathWorks, USA) was used to analyze whole brain voxel-wise imaging comparison ($p = 0.05$, cluster = 20 voxels) (Leiter et al., 2019).

2.6 | T-maze test

The T-maze test (central arm 46 × 11 × 10 cm; side arms 80 × 11 × 10 cm, dark-gray color) is based on the natural tendency of rodents to alternate between arms, exploring novel paths, which are considered an adaptive mechanism (d'Isa et al., 2021). The test was performed in an adjacent room under comparable environment conditions (temperature, humidity, light intensity, and cycle) to those of the housing room. Animals were kept in this room for at least 30 min prior to the test to allow for acclimatization. The floor and walls of the apparatus were thoroughly cleaned with a 70% ethanol solution and dried at the end of each use. Behaviors were videotaped to avoid the presence of the experimenter in the room. An experimenter blind to the experimental groups scored the behavioral variables.

Groups used in this experiment were KA + SAL ($n = 8$) and KA + CNO ($n = 7$). The experiments were performed at day 9 post KA injection, and consisted of a first trial, in which the animal was allowed to freely explore only one arm of the maze for 5 min while the other arm was kept closed, and a posttest 6 h later, in which the animal was placed at the starting point of the maze, this time with both arms open, to assess its interest in the previously unexplored arm. The time spent in each arm and the number of entries (all four paws) into each arm were evaluated. Ratios were then calculated for the percentage of time spent in the new unexplored arm or in the already explored one.

2.7 | Neurohistochemistry

At the end of the studies, animals were sacrificed, and the brains were collected and stored at −80°C. Brains were sliced coronally (30-μm thick) at the level of the hippocampus using a cryostat (Leica, Germany).

Immunofluorescence studies were performed to assess neuronal loss (NeuN), astrogliosis (GFAP) and to validate virus injection site. Slices were fixed with 4% formaldehyde in phosphate buffered saline (PBS) pH 7.4 for 10 min and washed with PBS (3 times, 3 min each). Then, they were rinsed in tris-buffered saline (TBS) for 30 min and blocked with 3% bovine serum albumin (BSA) (Sigma-Aldrich, Germany), 0.1% triton X-100 in TBS for 60 min. Slides were incubated at 4°C overnight with mouse Anti-GFAP antibody (1:500, Invitrogen, RRID AB10598515) or rabbit Anti-NeuN (1:500, Abcam, RRID AB177487, in 1% BSA/TBS). The next day, the sections for NeuN immunofluorescence were washed with 0.1% Tween 20 in TBS (3 × 5 min) and incubated with Goat Anti-Rabbit secondary antibody conjugated with Alexa Fluor® 488 (1:500, Abcam, RRID AB150077) for 1 h at room temperature. Finally, they were washed with 0.1% Tween 20 in TBS (3 × 5 min), adding in the last wash DAPI (1 mL of stock solution at 0.01% in TBS) to label the cell nuclei, and mounted directly with Mowiol. Sections were stored at 4°C, and images were acquired on a Leica SP5 (Leica, Germany) laser scanning confocal microscope or a Leitz Laborlux S microscope (Leica, Germany) with a FITC filter. For quantitative fluorescence analysis, FIJI-ImageJ software (NIH, available on the web: https://imagej.net/software/fiji/downloads) was used.

An ex vivo autoradiography was performed to assess the expression of the translocator protein (TSPO)-mediated neuroinflammation using the ^{3}H-PK11195 (Perkin Elmer, USA) as a marker of neuroinflammation as previously described (Slowing et al., 2023). Images were obtained by using a magnifying glass (Leica MZ6, Leica, Germany) attached to a digital camera. Images were analyzed with PMOD 4.2 software (PMOD Technologies, Switzerland) (Brackhan et al., 2016).

2.8 | Nuclear magnetic resonance spectroscopy

Hippocampal tissue was collected at day 9 after KA injection and chronic treatment with saline or CNO (KA + SAL $n = 8$; KA + CNO $n = 7$). ^{1}H-nuclear magnetic resonance (NMR) spectroscopy was performed in the ICTS Bioimagen Complutense (Universidad Complutense de Madrid, Spain) at 500.13 MHz using a Bruker AVIII500 HD spectrometer 11.7 T, as previously described (Llorente et al., 2012; Ruiz-Hurtado et al., 2017).

^{1}H, ^{13}C 2D experiments were performed to carry out the component's assignments. HMQC experiments were registered with the following parameters: 70 μs for GARP ^{13}C decoupling, 6009 and 22 kHz spectral widths in the ^{1}H and ^{13}C dimensions, respectively, 2 k data points in f2 and 256 increments in f1. Zero filling in f1 and unshifted squared sinusoidal window function in both dimensions were applied before Fourier transformation. In this study, multivariate statistical algorithms were used to classify high resolution magic angle spinning (HR-MAS) ^{1}H NMR spectra of these samples and identify distinct metabolic profiles for the different tissues. For pattern recognition analysis, ^{1}H NMR spectra were data reduced using the software program AMIX (Analysis of MIXtures version 3.6.8, Bruker Rheinstetten, Germany) by subdivision into integral regions of 0.02 ppm between δ 0.6 and 9 ppm (excluding the water region from 5.7 to 4.7 ppm). Individual integral regions were normalized to the total sum of integral regions following exclusion of the water resonance. Partial least squared (PLS) regression was applied to the data.

2.9 | Statistics

Data analyses were performed using the statistical program Graphpad Prism 6. Saphiro–Wilk normality test was used to assess the data normal distribution. For PET imaging analysis, the data were compared between experimental groups and its corresponding time points using a paired Student's *t*-test or repeated-measures one-way ANOVA with Bonferroni post hoc test (confidence interval 95%). Immunohistochemistry data were analyzed by two-way ANOVA with Tukey post hoc test (confidence interval 95%). We also analyzed each index in the kinetic model with comparison of treatments with their corresponding saline measure (*T*-test paired for repeated measures). Data are expressed as the mean ± standard error of the mean (SEM).

3 | RESULTS

3.1 | Astrocytic Ca^{2+} activation in WT mice resulted in brain glucose hypermetabolism

The presence of virus in the injection zone of the hippocampus was confirmed by histological analysis based on the colabeling of mCherry and GFAP in hippocampal astrocytes (Figure 1b).

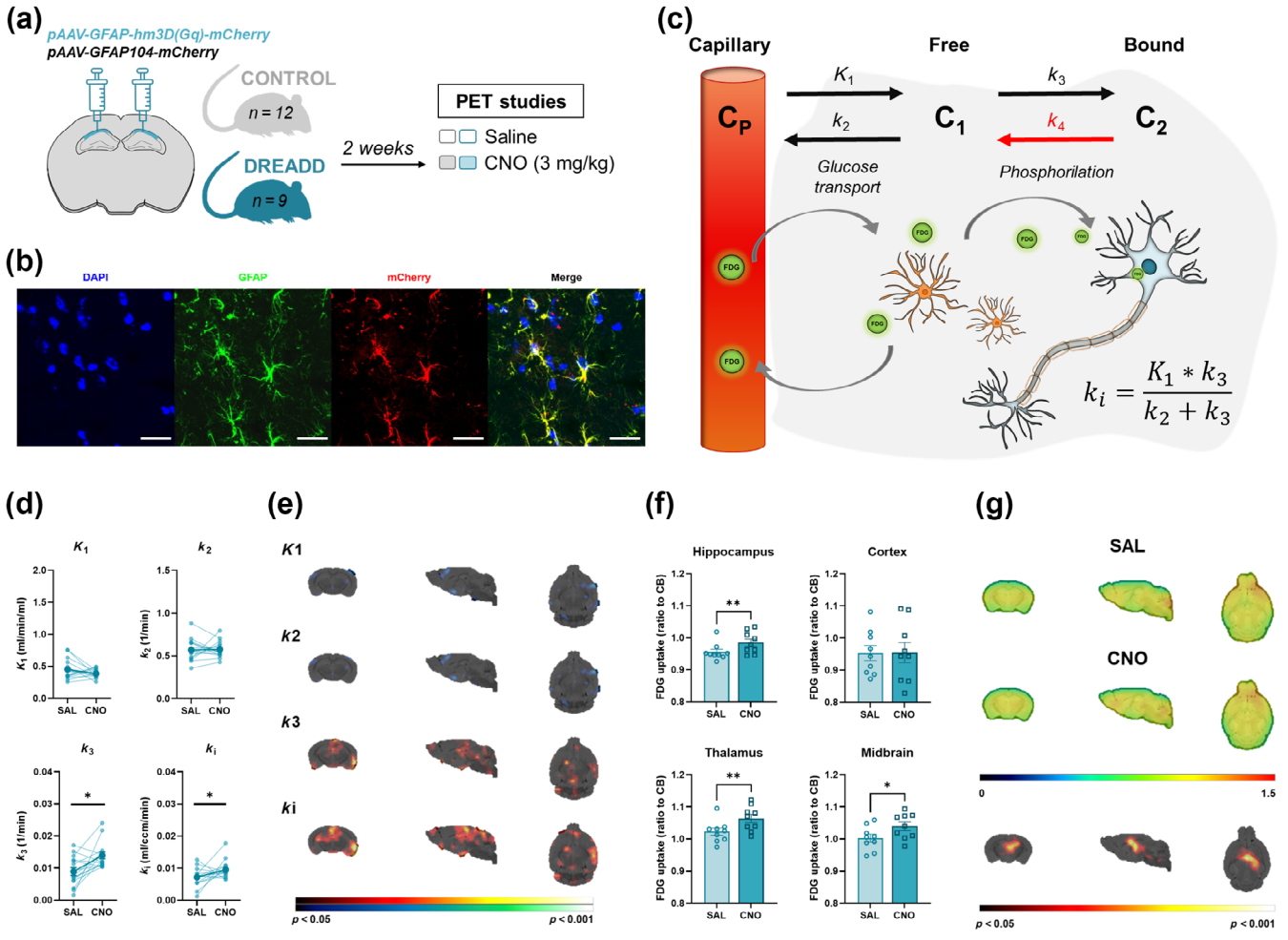

FIGURE 1 Astrocytic Ca^{2+} activation increases ^{18}F-FDG uptake. (a) Study design of surgeries, groups, and treatments. (b) Evidence of successful viral infection. Immunohistochemistry showed colocalization (yellow) between GFAP (astrocyte marker, green) and the fluorophore added to the viral vectors (mCherry, red) and DAPI (cell nuclei marker, blue). Scale bar at 20 μm. (c) Schematic representation of glucose kinetic constants in the 2TC model. The k_4 parameter is represented in red as $k_4 = 0$. (d) Graphs show that activation of astrocytes with CNO increased the value of the k_3 constant (SAL 0.009 ± 0.001 $n = 15$ vs. CNO 0.014 ± 0.001 $n = 15$; $p = 0.04$) and k_i, (SAL 0.007 ± 0.0008 $n = 15$ vs. CNO 0.1 ± 0.0007 $n = 15$; $p = 0.04$) indicating an increase in overall ^{18}F-FDG influx. Paired student's *t*-test, nonparametric. *$p < 0.05$. (e) SPM image representing the comparison between SAL and CNO of each constant, in which red and yellow areas represent a significant increase after treatment, and blue and green areas a decrease. (f) Graphs show quantification in several brain structures, where CNO causes a significant increase in ^{18}F-FDG uptake in hippocampus (SAL 0.9558 ± 0.02655 $n = 9$ vs. CNO 0.9848 ± 0.03387 $n = 9$; $p = 0.008$), thalamus (SAL 1.022 ± 0.03421 $n = 9$ vs. CNO 1.064 ± 0.039 $n = 9$; $p = 0.006$) and midbrain (SAL 1.002 ± 0.03744 $n = 9$ vs. CNO 1.040 ± 0.03928 $n = 9$; $p = 0.01$). Paired student's *t*-test. *$p < 0.05$; **$p < 0.01$. (g) Representation of mean images per treatment (top rows) and corresponding statistical comparison (bottom row) with SPM.

^{18}F-FDG dynamic studies (Figure 1c) showed that tracer influx (k_i) was higher in the WT/DREADD mice treated with CNO compared with the saline measure (Figure 1d,e). As expected, the WT/CONTROL group showed no differences in k_i after CNO treatment compared with saline (Figure S1). Static studies were performed to confirm this effect and to exclude any eventual effect of the anesthesia (awake radiotracer uptake). The results also showed an increase in ^{18}F-FDG uptake in the WT/DREADD mice treated with CNO. However, in this case, the hypermetabolism was not limited to the hippocampus, but it expanded to other brain areas such as the thalamus and midbrain (Figure 1f,g).

3.2 | Changes in glucose metabolism after astrocytic Ca^{2+} activation are mediated by GLUT1

The Ip3r2$^{-/-}$ mouse (Li et al., 2005) was employed as a negative control for astrocytic Ca^{2+} activation via chemogenetics, as the G protein-mediated astrocytic Ca^{2+} release from the endoplasmic reticulum in this animal is largely abolished (Corkrum et al., 2020; Martin-Fernandez et al., 2017; Petravicz et al., 2008). In Ip3r2$^{-/-}$ mice, dynamic studies showed no changes in glucose uptake kinetics after CNO administration (Figure 2a,b). These results were confirmed in static scans (Figure 2c,d), thus rejecting a possible masking effect of anesthesia.

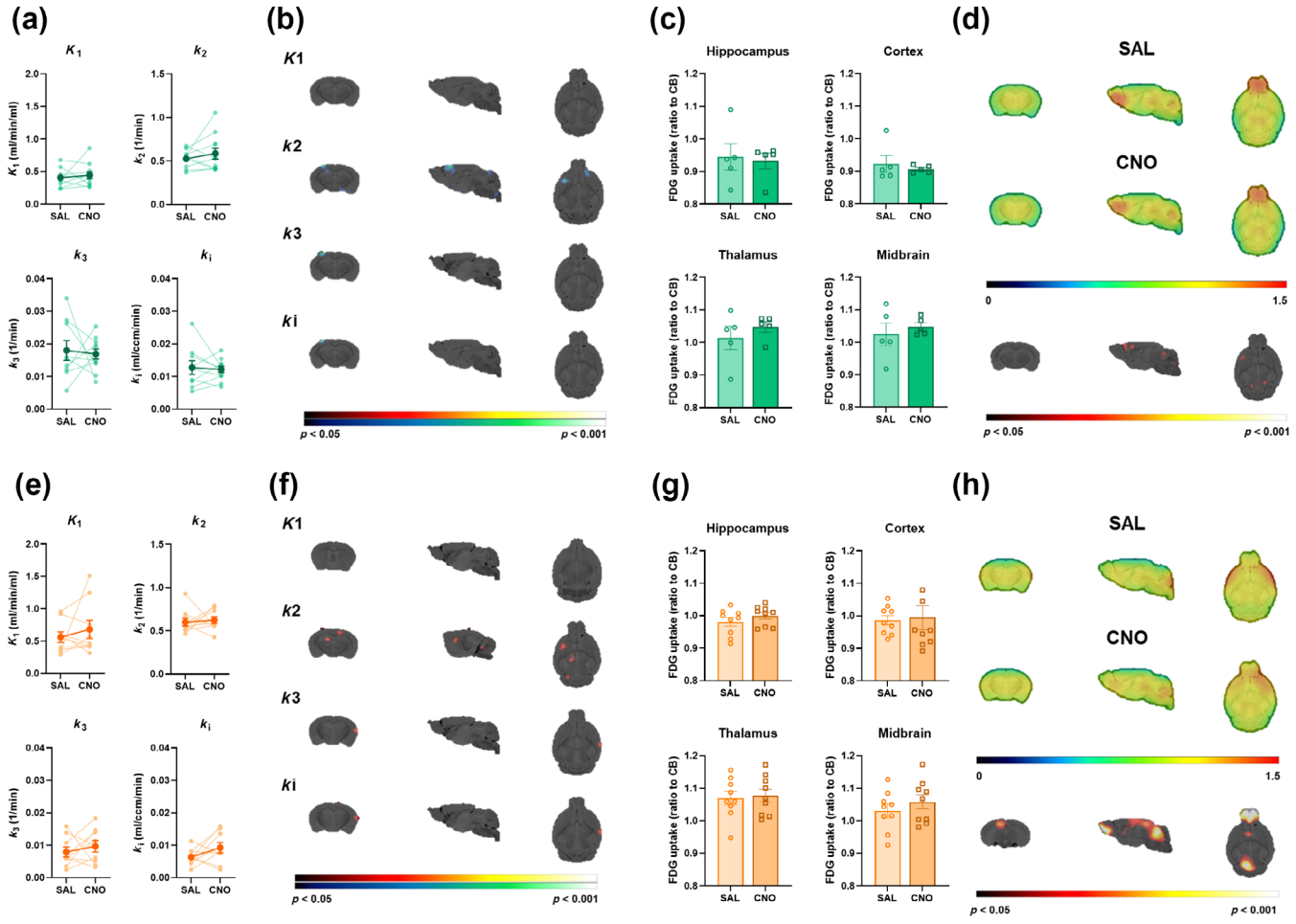

FIGURE 2 Metabolic changes in astrocyte activation are mediated glucose transporter GLUT1. (a) Dynamic PET graphs show that activation of astrocytes with CNO did not cause changes in any constant in Ip3r2$^{-/-}$ mice (SAL 0.014 ± 0.0034 $n = 5$ vs. CNO 0.010 ± 0.0011 $n = 5$; $p = 0.26$). Paired student's t-test. (b) Comparison of dynamic PET images of each constant, confirming no significant difference after treatment administration. (c) Static PET quantification in various brain structures showed no changes in glucose uptake after CNO administration in Ip3r2$^{-/-}$ mice (SAL 0.944 ± 0.0404 $n = 5$ vs. CNO 0.931 ± 0.0242 $n = 5$; $p > 0.99$). Paired student's t-test, nonparametric. (d) Static PET representation of the mean treatments (top rows) and their corresponding statistical comparison (bottom row), showing that the treatments behave similarly in Ip3r2$^{-/-}$ mice. (e) Activation of astrocytes with CNO in GLUT1$^{\Delta GFAP}$ mice did not cause changes in any constant in dynamic PET scans. (SAL 0.007 ± 0.0007 $n = 16$ vs. CNO 0.009 ± 0.005 $n = 16$; $p = 0.49$). Paired student's t-test. (f) SPM comparison of dynamic PET constants confirmed that there are no significant differences after treatment administration. (g) In static PET scans, graphs showed that CNO did not produce changes in glucose uptake in any of them (SAL 0.981 ± 0.0136 $n = 9$ vs. CNO 0.100 ± 0.0102 $n = 9$; $p = 0.13$). Paired student's t-test. (h) SPM representation of the static PET scans images and corresponding statistical comparison showed a significant increase in ^{18}F-FDG uptake when astrocytes are activated. However, the areas with the highest uptake correspond to the cerebral cortex and cerebellum, where there are no DREADDs that can respond to CNO.

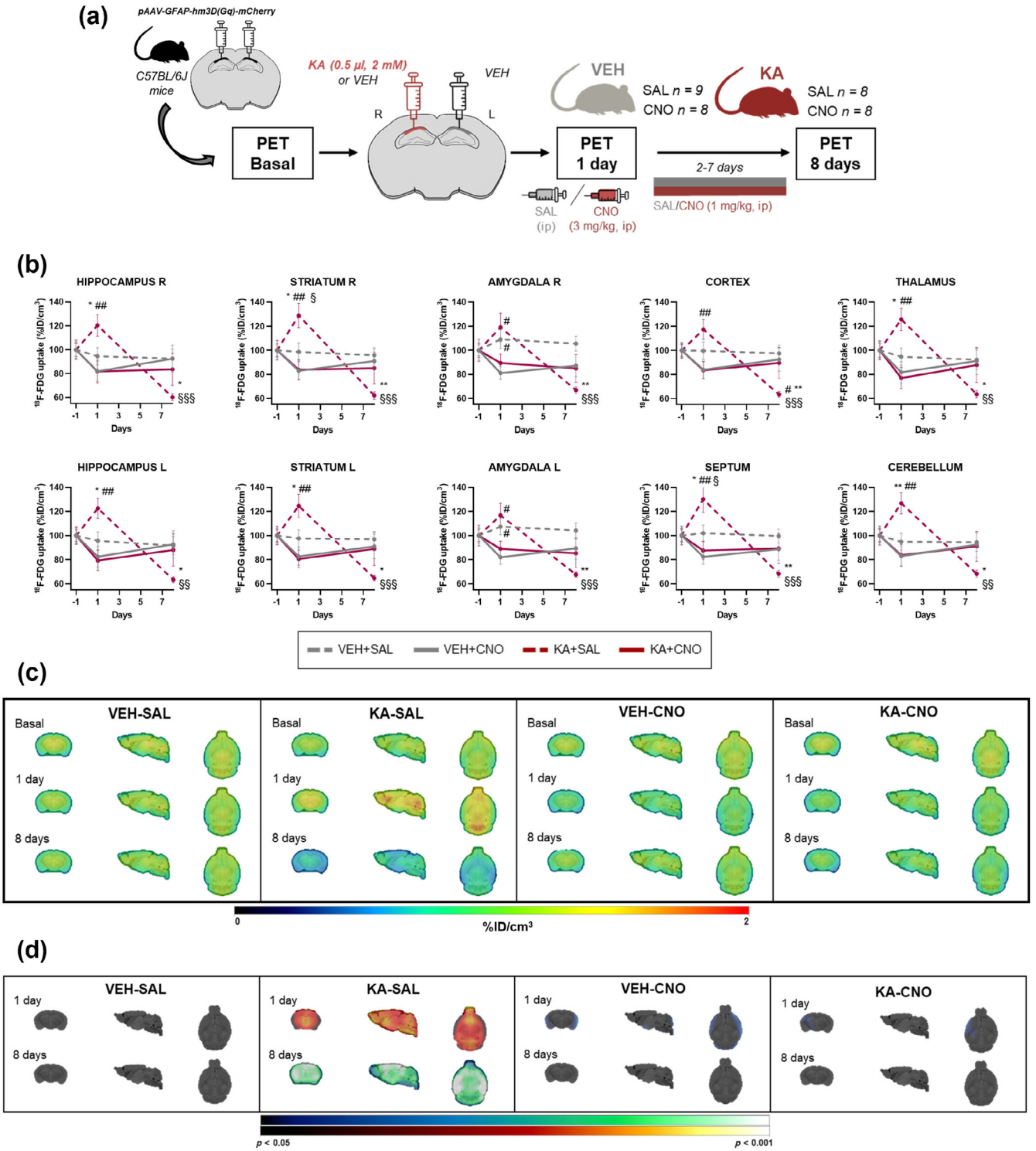

FIGURE 3 Astrocytic Ca^{2+} activation reverted metabolism in neurodegeneration. (a) Study design of surgeries, KA iHPC model induction, and imaging scans timeline. (b) Quantification of ^{18}F-FDG uptake (%ID/mL) showing significant differences in the KA + SAL group at day 1 (hippocampus: VEH + SAL 94.611% ± 7.251% $n = 9$ vs. KA + SAL 120.427% ± 9.152% $n = 7$; $p = 0.13$) and at day 8 (VEH + SAL 92.563% ± 7.712% $n = 9$ vs. KA + SAL 60.255% ± 2.723% $n = 7$; $p = 0.03$). However, these differences were not found in the CNO-treated group (day 1: VEH + CNO 81.902% ± 8.253% $n = 7$ vs. KA + CNO 81.828% ± 9.337% $n = 6$; $p > 0.99$; day 8: VEH + CNO 92.459% ± 11.341% $n = 7$ vs. KA + CNO 83.611% ± 13.43% $n = 6$; $p < 0.99$). Two-way ANOVA for repeated measures, post hoc Bonferroni. $^{*}p < 0.05$; $^{**}p < 0.01$; $^{***}p < 0.001$ SAL (VEH vs. KA); $^{\#}p < 0.05$; $^{\#\#}p < 0.01$; $^{\#\#\#}p < 0.001$ KA group (SAL vs. CNO); $^{\S}p < 0.05$; $^{\S\S}p < 0.01$; $^{\S\S\S\S}p < 0.001$ vs. baseline measurement. (c) Representative mean of ^{18}F-FDG PET images at different timeline. (d) Comparison of PET images with the baseline measurement, showing the increase (red) or decrease (blue) of metabolism. CNO, clozapine-N-oxide; iHPC, intrahippocampal; KA, kainic acid; PET, positron emission tomography; SAL, saline.

To test the role of astrocytes in glucose uptake, we used a genetically modified mice lacking GLUT1 in hippocampal astrocytes (GLUT1$^{\Delta GFAP}$). These animals showed no changes in ^{18}F-FDG uptake kinetics after CNO administration, as no differences were found on any constant of 2TC model or SPM comparison (Figure 2e,f). Same results were found in static PET scans, in which ^{18}F-FDG uptake was similar in all brain VOIs after both treatments (Figure 2g). Interestingly, SPM analysis showed a significant difference in subregions of cortex and cerebellum, but not in hippocampus (Figure 2h).

3.3 | Astrocytic Ca^{2+} activation rescued brain glucose metabolism in mice exposed to excitotoxicity induced by KA injection

We next investigate the role of astrocytes under conditions of damage induced by iHPC KA injection (Figure 3a). All animals reached the *status epilepticus* with a Racine scale score of 4–5.

The iHPC KA mouse model showed hypermetabolism 1 day after KA injection (KA + SAL) compared with its control group (VEH + SAL). Increased ^{18}F-FDG uptake was reversed by an acute injection of CNO (KA + CNO, 3 mg/kg, ip). Contrarily, a marked hypometabolism was found at day 8 in KA + SAL group compared with the basal measure. However, decreased ^{18}F-FDG uptake was not found after the sustained astrocytic Ca^{2+} activation during 7 days (KA + CNO) (Figure 3b–d). Moreover, the results of our study illustrate a discernible metabolic impact in the KA + SAL group, as evidenced by the emergence of hyperglycemia at day 8 postinjection (Figure S2A). However, no alterations in blood glucose levels were observed in the cohort treated with sustained astrocytic Ca^{2+} activation (KA + CNO). To ascertain whether the discrepancy in endogenous glucose levels and its competition with ^{18}F-FDG were influencing the actual brain metabolism, we conducted an analysis with the data corrected for blood glucose. The data exhibited a similar tendency to that observed in our previous analysis (Figure S2B), indicating that the effects of endogenous glucose and ^{18}F-FDG competition are not masking the impact of the astrocytic Ca^{2+} activation treatment.

We also studied the eventual changes in the metabolomic profile by ^{1}H-NMR spectroscopy. Interestingly, CNO-treated mice (KA + CNO group) showed higher concentrations of GABA compared with the KA + SAL in hippocampus (Figure S3A). Furthermore, multiple regression analysis by SPM showed a positive correlation between GABA levels and PET imaging in hippocampus, which was also confirmed by statistical multiple regression of VOI data (Figure S3B,C).

3.4 | Astrocytic Ca^{2+} activation prevented neuronal loss and recovered behavioral indexes of hippocampal function induced by excitotoxicity in iHPC KA mice

Because compromised hippocampal function by KA injection is known to alter behavior (Kim et al., 2017; Kumar et al., 2011; Miltiadous et al., 2013), we next evaluated the behavioral profile of these animals in the T-maze. The results showed that mice treated with CNO had a better performance. CNO-treated mice spent more time exploring the new-unexplored arm than those treated with saline. Similarly, the percentage of time spent in each arm in relation to the total time spent in both goal arms indicated that the astrocytic Ca^{2+} activation in the KA group spent a greater proportion of time in the new-unexplored arm than in the previously explored arm (Figure S4A,B).

We also assessed the impact of actrocytic activation at 9 days post iHPC KA injection, on various markers of neuronal viability and neuroinflammation. As expected, NeuN immunofluorescence signal was lower in the KA + SAL than in VEH + SAL group revealing that excitotoxicity induced by KA resulted in neuronal loss in hippocampus CA1 (Figure 4a,b). Interestingly, chronic astrocytic activation by CNO prevented the neuronal loss induced by KA.

Regarding GFAP immunofluorescence signal, both KA groups showed increased GFAP immunofluorescence signal in the hippocampus in a similar manner. Furthermore, astrocytic activation in VEH animals (VEH + CNO) resulted in a similar GFAP expression increase (Figure 4c,d).

When evaluating brain neuroinflammation by *ex vivo* TSPO autoradiography, our results showed that iHPC KA injection resulted in a significant increase in ^{3}H-PK11195 signal in KA + SAL mice when compared with the VEH + SAL group in multiple brain areas including hippocampus, cortex, thalamus, hypothalamus and amygdala. CNO-induced astrocytic activation by itself also resulted in a significant increase of ^{3}H-PK11195 signal in both hippocampi irrespective of KA- or VEH treatment (Figure 4e,f). However, sustained astrocytic Ca^{2+} activation reduced KA-induced TSPO expression in cerebral cortex and amygdala.

4 | DISCUSSION

In the present study, we used chemogenetics to investigate the effects of astrocytic Ca^{2+} activation on brain glucose metabolism, neuronal viability, markers of neuroinflammation, and glial reactivity and on behavioral aspects related to hippocampal functional state under an experimental pathological condition of brain damage induced by KA iHPC injection. To further deepen into the mechanisms underlying DREADD activation, we evaluated the potential involvement of astrocyte intracellular Ca^{2+} signaling mediated by Ip3r2 and the role of glucose exchange by the GLUT1. Herein, we show that astrocytic Ca^{2+} activation by itself results in brain glucose hypermetabolism, measured as ^{18}F-FDG uptake. In addition, our studies demonstrate that the functional integrity of both Ip3r2 and GLUT-1 are required for the effects of astrocytic Ca^{2+} activation in brain metabolism to occur. Furthermore, chronic astrocytic Ca^{2+} activation by CNO prevents the alterations induced by iHPC KA injection, having a protective role on neuronal viability and behavior impairment.

The effects of in vivo chemogenetics in neurons have been widely studied by evaluating their behavioral consequences both under normal and under neuropathological conditions such as in rat models of

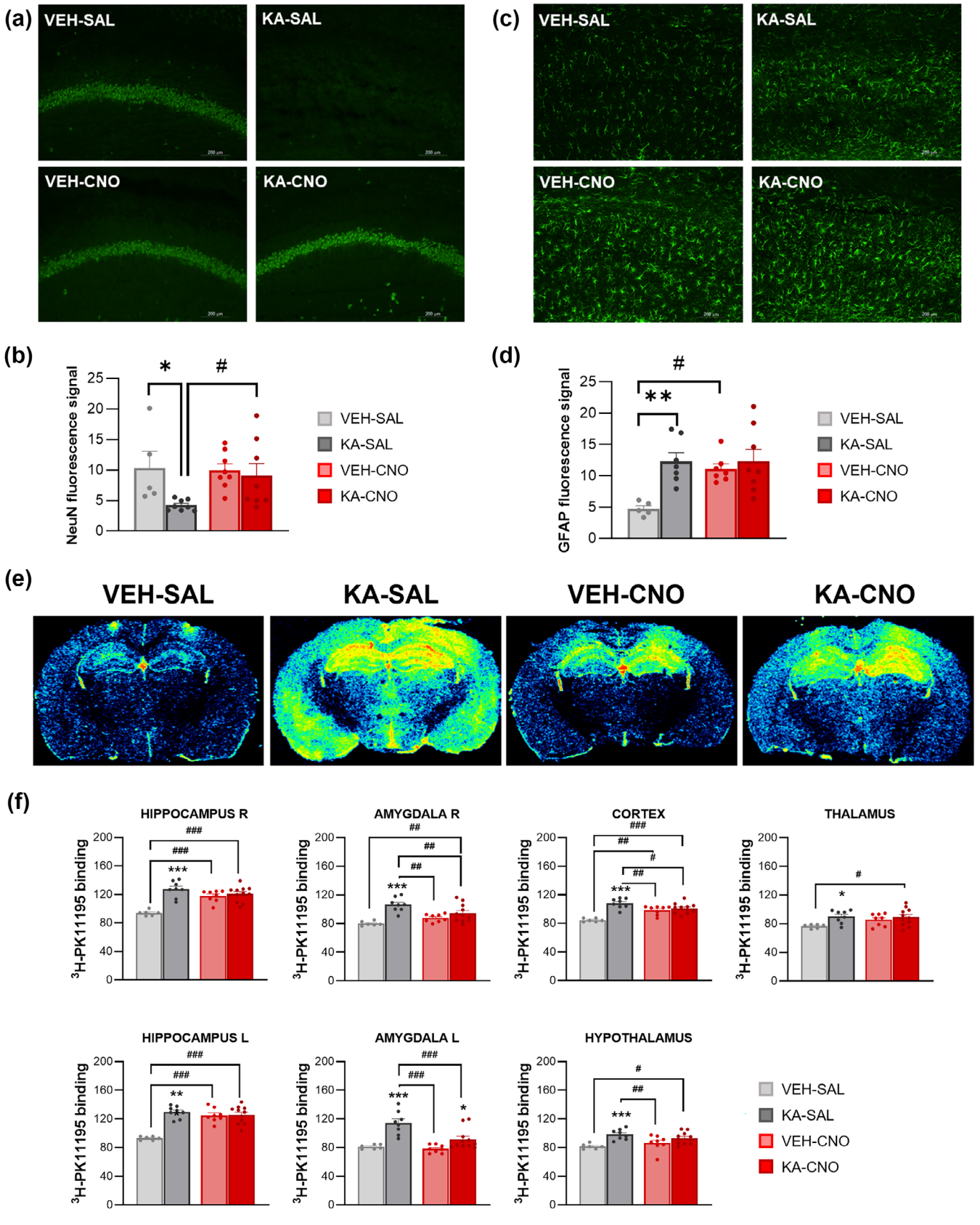

FIGURE 4 Legend on next page.

Alzheimer's disease or of temporal lobe epilepsy (Alami et al., 2020; Alcaraz et al., 2018; Goossens et al., 2019; Kang et al., 2020; Rorabaugh et al., 2017). Recent publications have shown that chemogenetic astrocytic activation also modulates cellular mechanisms and behaviors. (Jones et al., 2018; Lim et al., 2021; MacDonald et al., 2020; Nwachukwu et al., 2021) However, the brain glucose metabolic effects of in vivo astrocytic Ca^{2+} activation are not fully deciphered. To address this issue, we performed both dynamic and static ^{18}F-FDG PET scans to evaluate glucose uptake in the brain. Our findings indicate that astrocytic Ca^{2+} activation results in a measurable increase in brain glucose uptake. Our results add up to the evidence provided by other studies reporting that PET neuroimaging can indeed be a useful tool to evaluate changes in ^{18}F-FDG uptake mediated by nonneuronal cells (Rocha et al., 2022). Furthermore, the static PET scans showed that the increase in ^{18}F-FDG uptake is not only restricted to the hippocampus but also is observed in other brain regions distant from the injection site, extending beyond those expressing the DREADDs. This indicates that the metabolic effect induced by the activation of a subpopulation of astrocytes is not confined to the DREADD expression.

It is known that astrocytic activation results in an increase in the intracellular Ca^{2+} (Durkee et al., 2019), being the Ip3 the main mediator largely due to the activation of Gq-protein coupled receptors (Corkrum et al., 2020; Martin-Fernandez et al., 2017). Accordingly, we employed transgenic Ip3r2$^{-/-}$ mice, which exhibit astrocytes lacking the capacity to release Ca^{2+} release from the endoplasmic reticulum (Li et al., 2005) as negative control of astrocytic Ca^{2+} activation via chemogenetics. The results demonstrated that CNO injection in Ip3r2$^{-/-}$mice was unable to induce an increase in ^{18}F-FDG uptake. This evidence supports the conclusion that a functional Ip3r2-mediated intracellular Ca^{2+} signaling pathway is necessary for the manifestation of this metabolic effect.

Astrocytes are metabolically active and as we have shown, their activation contributes to changes in brain glucose metabolism measured by ^{18}F-FDG. Because astrocytes take up glucose via the GLUT1, we evaluated the involvement of GLUT1 on the ^{18}F-FDG increase seen after activation with DREADDs. Our results showed that astrocytic Ca^{2+} activation in GLUT1$^{\Delta GFAP}$ mice failed to induce glucose hypermetabolism in the hippocampus. However, we found differences when the radiotracer was injected in awake animals, but in areas where GLUT1 was conserved. Thus, GLUT1 is needed for ^{18}F-FDG uptake in astrocytes but not for astrocyte activation by DREADDS, as it modified glucose uptake in other brain areas. Nevertheless, alternative technical methodologies must be employed to ascertain whether the ^{18}F-FDG uptake is a result of neuronal or glial activity (Xiang et al., 2021). In vivo U-13C-glucose isotope tracing or cell sorting after ^{18}F-FDG injection may be effective approaches to elucidate the pathway followed by this tracer following astrocytic Ca^{2+} activation (Barros, Bolanos, et al., 2018; Rodrigues et al., 2013).

Once confirmed the metabolic effect of astrocytic Ca^{2+} activation by DREADDs, and considering that brain metabolic dysfunction (Blass, 2002) is a common features of many neurodegenerative diseases, we proceeded to evaluate the effect of astrocytic activation in a well-characterized model of excitotoxic damage induced by iHPC KA injection in mice (Lévesque & Avoli, 2013; Raedt et al., 2009; Riban et al., 2002). In line with previous studies, we found a significant hypermetabolism on day 1, followed by hypometabolism on day 8 (Bascuñana et al., 2020; García-García et al., 2016; Kornblum et al., 2000; Mirrione et al., 2006; Shiha et al., 2015). Interestingly, an acute dose of CNO 1 day after the insult was able to restore to basal the acute hypermetabolism induced by KA. Likewise, chronic CNO administration normalized the hypometabolism seen on day 8. Thus, our results show that activated astrocytes might play a pivotal role rescuing brain glucose metabolism after brain damage. Indeed, in alignment with prior research (Kim & Hong, 2015), KA elevated glycemia in the untreated cohort on day 8, whereas KA + CNO did not exhibit fluctuations in blood glucose levels relative to its baseline or other groups. This suggests that sustained astrocytic Ca^{2+} activation may also regulate hyperglycemia resulting from secondary effects of seizures, including increased cerebral metabolic rate (Fernandes et al., 1999) and glycolysis (Fray et al., 1997). The observed variation in endogenous glucose levels between the groups may potentially influence the competition with the ^{18}F-FDG uptake, thereby obscuring the actual brain metabolism. However, the analysis of ^{18}F-FDG uptake corrected for blood glucose levels yielded comparable results to those obtained without correction, thereby reinforcing the protective effect of astrocytic Ca^{2+} activation following KA injection.

In damaged brain areas, astrocytes experiment molecular and physiological changes that might be related to metabolic fluctuations and contribute to the development and progression of disease

FIGURE 4 Astrocytic Ca^{2+} activation prevented neuronal loss and neuroinflammation. (a) Immunofluorescent staining for NeuN in hippocampus CA1 in both control and KA-injected mice treated with saline or CNO on day 9 after SE. Scale bar: 200 μm. (b) NeuN immunofluorescent quantification showed that the KA + SAL group (4.211 ± 0.318 $n = 8$) had greater neuronal loss compared with VEH + SAL (10.321 ± 2.741 $n = 5$; $p = 0.02$) and KA + CNO (9.058 ± 1.976 $n = 8$; $p = 0.03$). Two-way ANOVA Fisher's LSD. (c) Immunofluorescent staining for GFAP in hippocampus CA1 in both control and KA-injected mice treated with saline or CNO on day 9 after SE. Scale bar: 200 μm. (d) GFAP immunofluorescence revealed significant differences between VEH + SAL control (4.724 ± 0.449 n = 5) and both KA-injected groups (KA + SAL 12.308 ± 1.361 $n = 7$; $p = 0.008$; KA + CNO 12.336 ± 1.85 $n = 8$; $p = 0.006$), but also in the control group treated with CNO (VEH + CNO 11.041 ± 0.834 $n = 7$; $p = 0.03$). Two-way ANOVA, post hoc Tukey. *$p < 0.05$; **$p < 0.01$. (e) Representative sample of ^{3}H-PK11195 uptake (TSPO) in coronal slice of the dorsal hippocampus. (f) Quantification of ^{3}H-PK11195 shows significant differences between VEH + SAL (94.088 ± 1.587 $n = 6$) and KA + SAL group (127.475 ± 4.043 $n = 8$; $p < 0.001$). The groups treated with CNO hardly showed any differences (VEH + CNO 117.836 ± 2.956 $n = 8$ vs. KA + CNO 120.638 ± 3.304 $n = 11$; $p = 0.92$). Two-way ANOVA, post hoc Tukey. *$p < 0.05$; **$p < 0.01$; ***$p < 0.001$. SAL, saline.

(Sofroniew & Vinters, 2010). Astrocytes are involved in a wide range of physiological functions including neuroinflammation, reactive gliosis, and glial scars related to sclerosis, which are associated with neuronal loss (Al Sufiani & Ang, 2012). Previous studies suggest that neuronal death might be the main responsible of hypometabolism found in several neurodegenerative diseases (Garcia-Garcia et al., 2023; García-García et al., 2016; Garibotto et al., 2017; Jeong et al., 2005; McKeith et al., 2017; Mosconi et al., 2009; Walker et al., 2018). Thus, it is likely that the neuronal death found on day 8 in the KA + SAL group (as detected by NeuN immunofluorescence) could be related, at least partially, with the hypometabolism found at this stage of the pathology. We also found that the sustained astrocytic Ca^{2+} activation during 7 days after iHPC KA resulted in preservation of neuronal survival in the CA1 hippocampal subregion, which consequently might have contributed to maintain brain glucose metabolism. Further, our NMR spectroscopy data showed that sustained astrocyte activation induced an increase in GABA levels in comparison with saline-treated animals. In addition, hippocampal GABA concentration was positively correlated with brain metabolism. This may indicate that astrocyte activation upregulates GABA concentration, inhibiting the glutamatergic neurons and thus preventing the neuronal death due to excitotoxicity.

Regarding our behavioral study, we show that KA + CNO group had better performance in T-maze than the KA + SAL. Even though we did not evaluated the effects of CNO by itself, several studies have shown that hippocampal astrocytes are involved in the generation of spatial cues during orientation (Doron et al., 2022), and that activation of these cells in that region is sufficient to enhance spatial memory (Adamsky et al., 2018). Our data suggest that the effect of sustained astrocytic Ca^{2+} activation on neuronal survival in the face of excitotoxic damage is also behaviorally reflected by restored hippocampal function.

As expected, GFAP signal was increased by the iHPC KA, an effect that persisted even after the activation of astrocyte cells in KA + CNO mice. Interestingly, the presence of GFAP expression in the VEH + CNO group in a similar level to KA + CNO may be attributed to the chemogenetic activation of these cells. Similar results were obtained in neuroinflammation measured by TSPO autoradiography. TSPO autoradiography in KA + SAL group showed a widespread expression in extra-hippocampal brain regions, as we reported previously after iHPC 4-aminopyridine injection (García-García et al., 2018). TSPO upregulation at 2 weeks has been demonstrated to possess prognostic capabilities, enabling the discrimination of the frequency of spontaneous seizures (Bertoglio et al., 2021). Prior research has indicated an increase in TSPO upregulation between 2 days and 7 weeks post-KA injection, a phenomenon that was also observed in the contralateral hippocampus and in the ipsilateral thalamus and cortex (Brackhan et al., 2018). Nevertheless, in KA + CNO mice, TSPO signal was reduced in cortex and amygdala, indicating that astrocytic Ca^{2+} activation resulted in a reduction of inflammation in these specific brain regions. Similar to GFAP results, TSPO was increased in VEH + CNO group. Our results reveal that sustained astrocytic Ca^{2+} activation induces overexpression of GFAP and TSPO on its own but may restrict neuroinflammation in other brain areas. Other researchers have identified a correlation between TSPO signal and microglia at 7–14 days postinjection, but with astrocytes at 6 months (Nguyen et al., 2018). This indicates that TSPO expression is associated with both glial cells, depending on the phase of epileptogenesis. Nevertheless, other studies have demonstrated that neuronal activity can independently alter TSPO levels in the brain (Notter et al., 2021). Consequently, TSPO expression can be augmented not only by sustained neuroinflammation but also by noninflammatory processes under specific physiological or pathological circumstances. Considering that the epileptic activity may be a potential cause of neuroinflammation in the brain, our hypothesis is that the astrocytic Ca^{2+} activation is limiting the epileptic activity that impacts sensitive brain regions as cortex and amygdala. Nevertheless, we cannot assure which mechanisms are directly involved in this TSPO reduction nor which cells are responsible for this decrease. Further research is needed to explore the implication of glial cells in the context of animal model of epilepsy, and the mechanisms involved in neuroinflammation restriction.

In conclusion, our study reveals that astrocyte Ca^{2+} activation by DREADDs increases brain glucose uptake and that both Ip3r2 and GLUT1 are key mediators in the underlying mechanisms. Further, in a pathological context, such as damage induced by iHPC KA, astrocyte activation had a significant role regulating brain glucose metabolism homeostasis. Furthermore, these metabolic effects were accompanied by beneficial effects preventing neuronal loss and increasing GABA levels in the hippocampus and protecting against brain neuroinflammation and behavioral alterations. Our findings sum up to other studies supporting the hypothesis that astrocyte activation may be a significant component of the neuroprotective mechanisms against brain damage, contributing to the maintenance of neuronal network integrity.

AUTHOR CONTRIBUTIONS

NH-M: Investigation, Formal analysis, Writing Original Draft - Review & Editing, Visualization; MGM: Investigation, Formal analysis; RFR: Investigation, Conceptualization, Methodology; LG-G and FG: Data Curation, Writing - Review & Editing; MS and PB: Investigation, Methodology, Writing - Review & Editing, Funding acquisition; MAP and EDM: Conceptualization, Methodology, Writing - Review & Editing, Supervision, Project administration, Funding acquisition.

FUNDING INFORMATION

This work was financially supported by Spanish Agencia Estatal de Investigación (AEI), Ministerio de Ciencia, Innovación y Universidades (MCIU) (AEI/10.13039/501100011033—M.A.P.: PDI2019-106968RB-100; E.D.M.: PID2020-116327GB-100; M.S.: SAF2017-87619-P). P.B. position is funded by a Miguel Servet grant (Instituto de Salud Carlos III, CP21/00020). N.H.M. position is funded by Alfonso Casanava fellowship granted by Universidad Complutense de Madrid. M.G.M. position was funded by Garantía Juvenil program granted by Comunidad de Madrid.

CONFLICT OF INTEREST STATEMENT

The authors declare no conflicts of interest.

DATA AVAILABILITY STATEMENT

The data that support the findings of this study are available on request from the corresponding author. The data are not publicly available due to privacy or ethical restrictions.

ORCID

Nira Hernández-Martín https://orcid.org/0009-0009-3933-1804

REFERENCES

Adamsky, A., Kol, A., Kreisel, T., Doron, A., Ozeri-Engelhard, N., Melcer, T., Refaeli, R., Horn, H., Regev, L., Groysman, M., London, M., & Goshen, I. (2018). Astrocytic activation generates De novo neuronal potentiation and memory enhancement. *Cell*, *174*, 59–71.e14. https://doi.org/10.1016/j.cell.2018.05.002

Al Sufiani, F., & Ang, L. C. (2012). Neuropathology of temporal lobe epilepsy. *Epilepsy Research and Treatment*, *2012*, 624519. https://doi.org/10.1155/2012/624519

Alami, N. O., Tang, L., Wiesner, D., Commisso, B., Bayer, D., Weishaupt, J., Dupuis, L., Wong, P., Baumann, B., Wirth, T., Boeckers, T. M., Yilmazer-Hanke, D., Ludolph, A., & Roselli, F. (2020). Multiplexed chemogenetics in astrocytes and motoneurons restore blood-spinal cord barrier in ALS. *Life Science Alliance*, *3*, 1–28.

Alcaraz, F., Fresno, V., Marchand, A. R., Kremer, E. J., Coutureau, E., & Wolff, M. (2018). Thalamocortical and corticothalamic pathways differentially contribute to goal-directed behaviors in the rat. *eLife*, *7*, e32517. https://doi.org/10.7554/eLife.32517

Andersen, J. V., Markussen, K. H., Jakobsen, E., Schousboe, A., Waagepetersen, H. S., Rosenberg, P. A., & Aldana, B. I. (2021). Glutamate metabolism and recycling at the excitatory synapse in health and neurodegeneration. *Neuropharmacology*, *196*, 108719. https://doi.org/10.1016/j.neuropharm.2021.108719

Andersen, J. V., McNair, L. F., Schousboe, A., & Waagepetersen, H. S. (2017). Specificity of exogenous acetate and glutamate as astrocyte substrates examined in acute brain slices from female mice using methionine sulfoximine (MSO) to inhibit glutamine synthesis. *Journal of Neuroscience Research*, *95*, 2207–2216. https://doi.org/10.1002/jnr.24038

Ardanaz, C. G., de la Cruz, A., Elizalde-Horcada, M., Puerta, E., Ramírez, M. J., Ortega, J. E., Urbiola, A., Ederra, C., Ariz, M., Ortiz-de-Solórzano, C., Fernández-Irigoyen, J., Santamaría, E., Karsenty, G., Brüning, J. C., & Solas, M. (2022). GLUT1 ablation in astrocytes paradoxically improves central and peripheral glucose metabolism via enhanced insulin-stimulated ATP release. bioRxiv: 2022.10.2006.511112 https://doi.org/10.1101/2022.10.06.511112

Attwell, D., Buchan, A. M., Charpak, S., Lauritzen, M., MacVicar, B. A., & Newman, E. A. (2010). Glial and neuronal control of brain blood flow. *Nature*, *468*, 232–243.

Barros, L. F., Bolanos, J. P., Bonvento, G., Bouzier-Sore, A. K., Brown, A., Hirrlinger, J., Kasparov, S., Kirchhoff, F., Murphy, A. N., Pellerin, L., Robinson, M. B., & Weber, B. (2018). Current technical approaches to brain energy metabolism. *Glia*, *66*, 1138–1159. https://doi.org/10.1002/glia.23248

Barros, L. F., Brown, A., & Swanson, R. A. (2018). Glia in brain energy metabolism: A perspective. *Glia*, *66*, 1134–1137. https://doi.org/10.1002/glia.23316

Bascuñana, P., Brackhan, M., Leiter, I., Keller, H., Jahreis, I., Ross, T. L., Bengel, F. M., Bankstahl, M., & Bankstahl, J. P. (2020). Divergent metabolic substrate utilization in brain during epileptogenesis precedes chronic hypometabolism. *Journal of Cerebral Blood Flow and Metabolism*, *40*, 204–213.

Bertoglio, D., Amhaoul, H., Goossens, J., Ali, I., Jonckers, E., Bijnens, T., Siano, M., Wyffels, L., Verhaeghe, J., van der Linden, A., Staelens, S., & Dedeurwaerdere, S. (2021). TSPO PET upregulation predicts epileptic phenotype at disease onset independently from chronic TSPO expression in a rat model of temporal lobe epilepsy. *Neuroimage Clinical*, *31*, 102701. https://doi.org/10.1016/j.nicl.2021.102701

Blass, J. P. (2002). Glucose/mitochondria in neurological conditions. *International Review of Neurobiology*, *51*, 325–376. https://doi.org/10.1016/s0074-7742(02)51010-2

Bonder, D. E., & McCarthy, K. D. (2014). Astrocytic Gq-GPCR-linked IP3R-dependent Ca2+ signaling does not mediate neurovascular coupling in mouse visual cortex in vivo. *The Journal of Neuroscience*, *34*, 13139–13150. https://doi.org/10.1523/JNEUROSCI.2591-14.2014

Brackhan, M., Bascunana, P., Postema, J. M., et al. (2016). Serial quantitative TSPO-targeted PET reveals peak microglial activation up to 2 weeks after an epileptogenic brain insult. *Journal of Nuclear Medicine*, *57*, 1302–1308. https://doi.org/10.2967/jnumed.116.172494

Brackhan, M., Bascunana, P., Ross, T. L., Bengel, F. M., Bankstahl, J. P., & Bankstahl, M. (2018). [(18) F]GE180 positron emission tomographic imaging indicates a potential double-hit insult in the intrahippocampal kainate mouse model of temporal lobe epilepsy. *Epilepsia*, *59*, 617–626. https://doi.org/10.1111/epi.14009

Brandebura, A. N., Paumier, A., Onur, T. S., & Allen, N. J. (2023). Astrocyte contribution to dysfunction, risk and progression in neurodegenerative disorders. *Nature Reviews. Neuroscience*, *24*, 23–39. https://doi.org/10.1038/s41583-022-00641-1

Carne, R. P., O'Brien, T. J., Kilpatrick, C. J., MacGregor, L. R., Hicks, R. J., Murphy, M. A., Bowden, S. C., Kaye, A. H., & Cook, M. J. (2004). MRI-negative PET-positive temporal lobe epilepsy: A distinct surgically remediable syndrome. *Brain*, *127*, 2276–2285. https://doi.org/10.1093/brain/awh257

Corkrum, M., Covelo, A., Lines, J., Bellocchio, L., Pisansky, M., Loke, K., Quintana, R., Rothwell, P. E., Lujan, R., Marsicano, G., Martin, E. D., Thomas, M. J., Kofuji, P., & Araque, A. (2020). Dopamine-evoked synaptic regulation in the nucleus accumbens requires astrocyte activity. *Neuron*, *105*, 1036–1047. https://doi.org/10.1016/j.neuron.2019.12.026

Danbolt, N. C., Furness, D. N., & Zhou, Y. (2016). Neuronal vs glial glutamate uptake: Resolving the conundrum. *Neurochemistry International*, *98*, 29–45. https://doi.org/10.1016/j.neuint.2016.05.009

Dave, A., Hansen, N., Downey, R., & Johnson, C. (2020). FDG-PET imaging of dementia and neurodegenerative disease. *Seminars in Ultrasound, CT, and MR*, *41*, 562–571. https://doi.org/10.1053/j.sult.2020.08.010

d'Isa, R., Comi, G., & Leocani, L. (2021). Apparatus design and behavioural testing protocol for the evaluation of spatial working memory in mice through the spontaneous alternation T-maze. *Scientific Reports*, *11*, 21177. https://doi.org/10.1038/s41598-021-00402-7

Doron, A., Rubin, A., Benmelech-Chovav, A., Benaim, N., Carmi, T., Refaeli, R., Novick, N., Kreisel, T., Ziv, Y., & Goshen, I. (2022). Hippocampal astrocytes encode reward location. *Nature*, *609*, 772–778. https://doi.org/10.1038/s41586-022-05146-6

Duncan, J. (2009). The current status of neuroimaging for epilepsy. *Current Opinion in Neurology*, *22*, 179–184. https://doi.org/10.1097/WCO.0b013e328328f260

Durkee, C. A., Covelo, A., Lines, J., Kofuji, P., Aguilar, J., & Araque, A. (2019). G(i/o) protein-coupled receptors inhibit neurons but activate astrocytes and stimulate gliotransmission. *Glia*, *67*, 1076–1093. https://doi.org/10.1002/glia.23589

Fernandes, M. J., Dube, C., Boyet, S., Marescaux, C., & Nehlig, A. (1999). Correlation between hypermetabolism and neuronal damage during status epilepticus induced by lithium and pilocarpine in immature and adult rats. *Journal of Cerebral Blood Flow and Metabolism*, *19*, 195–209. https://doi.org/10.1097/00004647-199902000-00011

Fray, A. E., Boutelle, M., & Fillenz, M. (1997). Extracellular glucose turnover in the striatum of unanaesthetized rats measured by quantitative microdialysis. *The Journal of Physiology*, *504*(Pt 3), 721–726. https://doi.org/10.1111/j.1469-7793.1997.721bd.x

García-García, L., Fernández de la Rosa, R., Delgado, M., Silván, Á., Bascuñana, P., Bankstahl, J. P., Gomez, F., & Pozo, M. A. (2018).

Metyrapone prevents acute glucose hypermetabolism and short-term brain damage induced by intrahippocampal administration of 4-aminopyridine in rats. *Neurochemistry International*, *113*, 92–106.

Garcia-Garcia, L., Gomez, F., Delgado, M., de la Rosa, R. F., & Pozo, M. Á. (2023). The vasodilator naftidrofuryl attenuates short-term brain glucose hypometabolism in the lithium-pilocarpine rat model of status epilepticus without providing neuroprotection. *European Journal of Pharmacology*, *939*, 175453. https://doi.org/10.1016/j.ejphar.2022.175453

García-García, L., Shiha, A. A., Bascuñana, P., de Cristóbal, J., Fernández de la Rosa, R., Delgado, M., & Pozo, M. A. (2016). Serotonin depletion does not modify the short-term brain hypometabolism and hippocampal neurodegeneration induced by the lithium–pilocarpine model of status epilepticus in rats. *Cellular and Molecular Neurobiology*, *36*, 513–519. https://doi.org/10.1007/s10571-015-0240-4

Garibotto, V., Herholz, K., Boccardi, M., Picco, A., Varrone, A., Nordberg, A., Nobili, F., Ratib, O., & Geneva Task Force for the Roadmap of Alzheimer's Biomarkers. (2017). Clinical validity of brain fluorodeoxyglucose positron emission tomography as a biomarker for Alzheimer's disease in the context of a structured 5-phase development framework. *Neurobiology of Aging*, *52*, 183–195. https://doi.org/10.1016/j.neurobiolaging.2016.03.033

Goossens, M.-G., Christiaen, E., Boon, P., Vonck, K., Carrette, E., Desloovere, J., van den Haute, C., Baekelandt, V., Wadman, W., Vanhove, C., & Raedt, R. (2019). Chemogenetic suppression of spontaneous seizures in a rat model for temporal lobe epilepsy. *Frontiers in Neuroscience*, *13*, 1–11.

Gordon, G. R. J., Mulligan, S. J., & MacVicar, B. A. (2007). Astrocyte control of the cerebrovasculature. *Glia*, *55*, 1214–1221.

Hynd, M. R., Scott, H. L., & Dodd, P. R. (2004). Glutamate-mediated excitotoxicity and neurodegeneration in Alzheimer's disease. *Neurochemistry International*, *45*, 583–595. https://doi.org/10.1016/j.neuint.2004.03.007

Iovino, L., Tremblay, M. E., & Civiero, L. (2020). Glutamate-induced excitotoxicity in Parkinson's disease: The role of glial cells. *Journal of Pharmacological Sciences*, *144*, 151–164. https://doi.org/10.1016/j.jphs.2020.07.011

Jeong, Y., Cho, S. S., Park, J. M., Kang, S. J., Lee, J. S., Kang, E., Na, D. L., & Kim, S. E. (2005). 18F-FDG PET findings in frontotemporal dementia: An SPM analysis of 29 patients. *Journal of Nuclear Medicine*, *46*, 233–239.

Jones, M. E., Paniccia, J. E., Lebonville, C. L., Reissner, K. J., & Lysle, D. T. (2018). Chemogenetic manipulation of dorsal hippocampal astrocytes protects against the development of stress-enhanced fear learning. *Neuroscience*, *388*, 45–56. https://doi.org/10.1016/j.neuroscience.2018.07.015

Kang, S., Hong, S. I., Lee, J., Peyton, L., Baker, M., Choi, S., Kim, H., Chang, S.-Y., & Choi, D.-S. (2020). Activation of astrocytes in the dorsomedial striatum facilitates transition from habitual to goal-directed reward-seeking behavior. *Biological Psychiatry*, *88*, 797–808.

Kim, C. H., & Hong, J. S. (2015). Intracerebroventricular kainic acid-induced damage affects blood glucose level in d-glucose-fed mouse model. *Experimental Neurobiolody*, *24*, 24–30. https://doi.org/10.5607/en.2015.24.1.24

Kim, S., Jung, U. J., Oh, Y. S., Jeon, M. T., Kim, H. J., Shin, W. H., Hong, J., & Kim, S. R. (2017). Beneficial effects of Silibinin against kainic acid-induced neurotoxicity in the hippocampus in vivo. *Experimental Neurobiology*, *26*, 266–277. https://doi.org/10.5607/en.2017.26.5.266

Kornblum, H. I., Araujo, D. M., Annala, A. J., Tatsukawa, K. J., Phelps, M. E., & Cherry, S. R. (2000). In vivo imaging of neuronal activation and plasticity in the rat brain by high resolution positron emission tomography (microPET). *Nature Biotechnology*, *18*, 655–660. https://doi.org/10.1038/76509

Kumar, A., Prakash, A., & Pahwa, D. (2011). Galantamine potentiates the protective effect of rofecoxib and caffeic acid against intrahippocampal kainic acid-induced cognitive dysfunction in rat. *Brain Research Bulletin*, *85*, 158–168. https://doi.org/10.1016/j.brainresbull.2011.03.010

Leiter, I., Bascunana, P., Bengel, F. M., Bankstahl, J. P., & Bankstahl, M. (2019). Attenuation of epileptogenesis by 2-deoxy-d-glucose is accompanied by increased cerebral glucose supply, microglial activation and reduced astrocytosis. *Neurobiology of Disease*, *130*, 104510. https://doi.org/10.1016/j.nbd.2019.104510

Lévesque, M., & Avoli, M. (2013). The kainic acid model of temporal lobe epilepsy. *Neuroscience and Biobehavioral Reviews*, *37*, 2887–2899.

Li, X., Zima, A. V., Sheikh, F., Blatter, L. A., & Chen, J. (2005). Endothelin-1-induced arrhythmogenic Ca2+ signaling is abolished in atrial myocytes of inositol-1,4,5-trisphosphate(IP3)-receptor type 2-deficient mice. *Circulation Research*, *96*, 1274–1281. https://doi.org/10.1161/01.RES.0000172556.05576.4c

Lim, E. Y., Ye, L., & Paukert, M. (2021). Potential and realized impact of astroglia Ca2 + dynamics on circuit function and behavior. *Frontiers in Cellular Neuroscience*, *15*, 1–19.

Llorente, R., Villa, P., Marco, E. M., & Viveros, M. P. (2012). Analyzing the effects of a single episode of neonatal maternal deprivation on metabolite profiles in rat brain: A proton nuclear magnetic resonance spectroscopy study. *Neuroscience*, *201*, 12–19. https://doi.org/10.1016/j.neuroscience.2011.11.033

Ma, Y., Hof, P. R., Grant, S. C., Blackband, S. J., Bennett, R., Slatest, L., McGuigan, M. D., & Benveniste, H. (2005). A three-dimensional digital atlas database of the adult C57BL/6J mouse brain by magnetic resonance microscopy. *Neuroscience*, *135*, 1203–1215. https://doi.org/10.1016/j.neuroscience.2005.07.014

MacDonald, A. J., Holmes, F. E., Beall, C., Pickering, A. E., & Ellacott, K. L. J. (2020). Regulation of food intake by astrocytes in the brainstem dorsal vagal complex. *Glia*, *68*, 1241–1254.

Marina, N., Turovsky, E., Christie, I. N., Hosford, P. S., Hadjihambi, A., Korsak, A., Ang, R., Mastitskaya, S., Sheikhbahaei, S., Theparambil, S. M., & Gourine, A. V. (2018). Brain metabolic sensing and metabolic signaling at the level of an astrocyte. *Glia*, *66*, 1185–1199.

Martin-Fernandez, M., Jamison, S., Robin, L. M., Zhao, Z., Martin, E. D., Aguilar, J., Benneyworth, M. A., Marsicano, G., & Araque, A. (2017). Synapse-specific astrocyte gating of amygdala-related behavior. *Nature Neuroscience*, *20*, 1540–1548. https://doi.org/10.1038/nn.4649

McKeith, I. G., Boeve, B. F., Dickson, D. W., Halliday, G., Taylor, J. P., Weintraub, D., Aarsland, D., Galvin, J., Attems, J., Ballard, C. G., Bayston, A., Beach, T. G., Blanc, F., Bohnen, N., Bonanni, L., Bras, J., Brundin, P., Burn, D., Chen-Plotkin, A., … Kosaka, K. (2017). Diagnosis and management of dementia with Lewy bodies: Fourth consensus report of the DLB consortium. *Neurology*, *89*, 88–100. https://doi.org/10.1212/WNL.0000000000004058

Meyer, P. T., Frings, L., Rucker, G., & Hellwig, S. (2017). (18)F-FDG PET in parkinsonism: Differential diagnosis and evaluation of cognitive impairment. *Journal of Nuclear Medicine*, *58*, 1888–1898. https://doi.org/10.2967/jnumed.116.186403

Miltiadous, P., Kouroupi, G., Stamatakis, A., Koutsoudaki, P. N., Matsas, R., & Stylianopoulou, F. (2013). Subventricular zone-derived neural stem cell grafts protect against hippocampal degeneration and restore cognitive function in the mouse following intrahippocampal kainic acid administration. *Stem Cells Translational Medicine*, *2*, 185–198. https://doi.org/10.5966/sctm.2012-0074

Mirrione, M. M., Schiffer, W. K., Siddiq, M., Dewey, S. L., & Tsirka, S. E. (2006). PET imaging of glucose metabolism in a mouse model of temporal lobe epilepsy. *Synapse*, *59*, 119–121.

Mosconi, L., Mistur, R., Switalski, R., Tsui, W. H., Glodzik, L., Li, Y., Pirraglia, E., de Santi, S., Reisberg, B., Wisniewski, T., & de Leon, M. J.

(2009). FDG-PET changes in brain glucose metabolism from normal cognition to pathologically verified Alzheimer's disease. *European Journal of Nuclear Medicine and Molecular Imaging*, *36*, 811–822. https://doi.org/10.1007/s00259-008-1039-z

Nguyen, D. L., Wimberley, C., Truillet, C., Jego, B., Caillé, F., Pottier, G., Boisgard, R., Buvat, I., & Bouilleret, V. (2018). Longitudinal positron emission tomography imaging of glial cell activation in a mouse model of mesial temporal lobe epilepsy: Toward identification of optimal treatment windows. *Epilepsia*, *59*, 1234–1244. https://doi.org/10.1111/epi.14083

Notter, T., Schalbetter, S. M., Clifton, N. E., Mattei, D., Richetto, J., Thomas, K., Meyer, U., & Hall, J. (2021). Neuronal activity increases translocator protein (TSPO) levels. *Molecular Psychiatry*, *26*, 2025–2037. https://doi.org/10.1038/s41380-020-0745-1

Nwachukwu, K. N., Evans, W. A., Sides, T. R., Trevisani, C. P., Davis, A., & Marshall, S. A. (2021). Chemogenetic manipulation of astrocytic signaling in the basolateral amygdala reduces binge-like alcohol consumption in male mice. *Journal of Neuroscience Research*, *99*, 1957–1972.

Olney, J. W. (1971). Glutamate-induced neuronal necrosis in the infant mouse hypothalamus. An electron microscopic study. *Journal of Neuropathology and Experimental Neurology*, *30*, 75–90. https://doi.org/10.1097/00005072-197101000-00008

Petravicz, J., Fiacco, T. A., & McCarthy, K. D. (2008). Loss of IP3 receptor-dependent Ca2+ increases in hippocampal astrocytes does not affect baseline CA1 pyramidal neuron synaptic activity. *The Journal of Neuroscience*, *28*, 4967–4973. https://doi.org/10.1523/JNEUROSCI.5572-07.2008

Provenzano, F., Torazza, C., Bonifacino, T., Bonanno, G., & Milanese, M. (2023). The key role of astrocytes in amyotrophic lateral sclerosis and their commitment to glutamate excitotoxicity. *International Journal of Molecular Sciences*, *24*, 15430. https://doi.org/10.3390/ijms242015430

Qian, Y., Guan, T., Tang, X., Huang, L., Huang, M., Li, Y., Sun, H., Yu, R., & Zhang, F. (2011). Astrocytic glutamate transporter-dependent neuroprotection against glutamate toxicity: An in vitro study of maslinic acid. *European Journal of Pharmacology*, *651*, 59–65. https://doi.org/10.1016/j.ejphar.2010.10.095

Racine, R. J. (1972). Modification of seizure activity by electrical stimulation. II. Motor seizure. *Electroencephalography and Clinical Neurophysiology*, *32*, 281–294. https://doi.org/10.1016/0013-4694(72)90177-0

Raedt, R., Van Dycke, A., Van Melkebeke, D., Bouzier-Sore, A. K., Brown, A., Hirrlinger, J., Kasparov, S., Kirchhoff, F., Murphy, A. N., Pellerin, L., Robinson, M. B., & Weber, B. (2009). Seizures in the intrahippocampal kainic acid epilepsy model: Characterization using long-term video-EEG monitoring in the rat. *Acta Neurologica Scandinavica*, *119*, 293–303. https://doi.org/10.1111/j.1600-0404.2008.01108.x

Riban, V., Bouilleret, V., Pham-Le, B. T., Fritschy, J.-M., Marescaux, C., & Depaulis, A. (2002). Evolution of hippocampal epileptic activity during the development of hippocampal sclerosis in a mouse model of temporal lobe epilepsy. *Neuroscience*, *112*, 101–111. https://doi.org/10.1016/s0306-4522(02)00064-7

Rocha, A., Bellaver, B., Souza, D. G., Schu, G., Fontana, I. C., Venturin, G. T., Greggio, S., Fontella, F. U., Schiavenin, M. L., Machado, L. S., Miron, D., da Costa, J. C., Rosa-Neto, P., Souza, D. O., Pellerin, L., & Zimmer, E. R. (2022). Clozapine induces astrocyte-dependent FDG-PET hypometabolism. *European Journal of Nuclear Medicine and Molecular Imaging*, *49*, 2251–2264. https://doi.org/10.1007/s00259-022-05682-3

Rodrigues, T. B., Valette, J., & Bouzier-Sore, A. K. (2013). (13)C NMR spectroscopy applications to brain energy metabolism. *Frontiers in Neuroenergetics*, *5*, 9. https://doi.org/10.3389/fnene.2013.00009

Rorabaugh, J. M., Chalermpalanupap, T., Botz-Zapp, C. A., Fu, V. M., Lembeck, N. A., Cohen, R. M., & Weinshenker, D. (2017). Chemogenetic locus coeruleus activation restores reversal learning in a rat model of Alzheimer's disease. *Brain*, *140*, 3023–3038. https://doi.org/10.1093/brain/awx232

Ruiz-Hurtado, G., Garcia-Prieto, C. F., Pulido-Olmo, H., Velasco-Martín, J. P., Villa-Valverde, P., Fernández-Valle, M. E., Boscá, L., Fernández-Velasco, M., Regadera, J., Somoza, B., & Fernández-Alfonso, M. S. (2017). Mild and short-term caloric restriction prevents obesity-induced cardiomyopathy in young Zucker rats without changing in metabolites and fatty acids cardiac profile. *Frontiers in Physiology*, *8*, 42. https://doi.org/10.3389/fphys.2017.00042

Sepers, M. D., & Raymond, L. A. (2014). Mechanisms of synaptic dysfunction and excitotoxicity in Huntington's disease. *Drug Discovery Today*, *19*, 990–996. https://doi.org/10.1016/j.drudis.2014.02.006

Shen, W., Chen, S., Liu, Y., Han, P., Ma, T., & Zeng, L. H. (2021). Chemogenetic manipulation of astrocytic activity: Is it possible to reveal the roles of astrocytes? *Biochemical Pharmacology*, *186*, 114457.

Shiha, A. A., de Cristóbal, J., Delgado, M., Fernández de la Rosa, R., Bascuñana, P., Pozo, M. A., & García-García, L. (2015). Subacute administration of fluoxetine prevents short-term brain hypometabolism and reduces brain damage markers induced by the lithium-pilocarpine model of epilepsy in rats. *Brain Research Bulletin*, *111*, 36–47.

Slowing, K., Gomez, F., Delgado, M., Fernández de la Rosa, R., Hernández-Martín, N., Pozo, M. Á., & García-García, L. (2023). PET imaging and neurohistochemistry reveal that curcumin attenuates brain hypometabolism and hippocampal damage induced by status epilepticus in rats. *Planta Medica*, *89*, 364–376. https://doi.org/10.1055/a-1948-4378

Sofroniew, M. V., & Vinters, H. V. (2010). Astrocytes: Biology and pathology. *Acta Neuropathologica*, *119*, 7–35. https://doi.org/10.1007/s00401-009-0619-8

Stoklund Dittlau, K., & Freude, K. (2024). Astrocytes: The stars in neurodegeneration? *Biomolecules*, *14*, 289. https://doi.org/10.3390/biom14030289

Walker, Z., Gandolfo, F., Orini, S., Garibotto, V., Agosta, F., Arbizu, J., Bouwman, F., Drzezga, A., Nestor, P., Boccardi, M., Altomare, D., Festari, C., Nobili, F., & EANM-EAN task force for the recommendation of FDG PET for dementing neurodegenerative disorders. (2018). Clinical utility of FDG PET in Parkinson's disease and atypical parkinsonism associated with dementia. *European Journal of Nuclear Medicine and Molecular Imaging*, *45*, 1534–1545. https://doi.org/10.1007/s00259-018-4031-2

Xiang, X., Wind, K., Wiedemann, T., Blume, T., Shi, Y., Briel, N., Beyer, L., Biechele, G., Eckenweber, F., Zatcepin, A., Lammich, S., Ribicic, S., Tahirovic, S., Willem, M., Deussing, M., Palleis, C., Rauchmann, B. S., Gildehaus, F. J., Lindner, S., … Brendel, M. (2021). Microglial activation states drive glucose uptake and FDG-PET alterations in neurodegenerative diseases. *Science Translational Medicine*, *13*, eabe5640. https://doi.org/10.1126/scitranslmed.abe5640

SUPPORTING INFORMATION

Additional supporting information can be found online in the Supporting Information section at the end of this article.

How to cite this article: Hernández-Martín, N., Martínez, M. G., Bascuñana, P., Fernández de la Rosa, R., García-García, L., Gómez, F., Solas, M., Martín, E. D., & Pozo, M. A. (2024). Astrocytic Ca^{2+} activation by chemogenetics mitigates the effect of kainic acid-induced excitotoxicity on the hippocampus. *Glia*, *72*(12), 2217–2230. https://doi.org/10.1002/glia.24607